

# *XMM-Newton* Observations of the TeV $\gamma$ -ray Source HESS J1804-216

Dacheng Lin<sup>1,2</sup>, Natalie A. Webb<sup>1,2</sup>, Didier Barret<sup>1,2</sup>

## ABSTRACT

We have analyzed three *XMM-Newton* observations of the central part of the unidentified TeV  $\gamma$ -ray source HESS J1804-216. We focus on two X-ray sources 2XMMi J180442.0-214221 (Src 1) and 2XMMi J180432.5-214009 (Src 2), which were suggested to be the possible X-ray counterparts to the TeV source. We discover a 2.93 hr X-ray periodicity from Src 1, with the pulse profile explained with a self-eclipsing pole in an eclipsing polar. Src 2 exhibits a strong Fe emission line (FWHM  $\sim 0.3$  keV and equivalent width  $\sim 0.8$  keV) and large X-ray variability on timescales of hours and is probably an intermediate polar. Thus Src 1 and Src 2 are probably two field sources not responsible for the TeV emission. The observations were contaminated by strong straylight from a nearby bright source, and we see no clear extended X-ray emission that can be attributed to the supernova remnant G8.7-0.1, a popular possible association with the TeV source. The other possible association, the pulsar wind nebula candidate PSR J1803-2137, shows little long-term variability, compared with a previous *Chandra* observation. Many point sources were serendipitously detected, but most of them are probably normal stars. Three new candidate compact object systems (other than Src 1, Src 2 and PSR J1803-2137) are also found. They are far away from the TeV source and are probably also magnetic cataclysmic variables, thus unlikely to be responsible for the TeV emission.

*Subject headings:* acceleration of particles — gamma rays: ISM — X-rays: individual (2XMMi J180442.0-214221, 2XMMi J180432.5-214009, PSR J1803-2137, HESS J1804-216, G8.7-0.1)

---

<sup>1</sup>CNRS, IRAP, 9 avenue du Colonel Roche, BP 44346, F-31028 Toulouse Cedex 4, France, email: Dacheng.Lin@irap.omp.eu

<sup>2</sup>Université de Toulouse, UPS-OMP, IRAP, Toulouse, France

## 1. INTRODUCTION

More than 100 TeV  $\gamma$ -ray sources have been discovered<sup>1</sup> (See Hinton & Hofmann 2009, for a recent review). About 60 of them, all probably Galactic, have no firm associations at other wavelengths. HESS J1804-216 is the brightest among these unidentified TeV  $\gamma$ -ray sources, with a flux above 200 GeV around  $5.3 \times 10^{-11}$  erg s<sup>-1</sup> cm<sup>-2</sup> (nearly 25% of the Crab Nebula). It was discovered by the High Energy Stereoscopic System (H.E.S.S.) in 2004, with the best-fit position of  $l=8.401^\circ \pm 0.016^\circ$  and  $b=-0.033^\circ \pm 0.018^\circ$  in Galactic coordinates (Aharonian et al. 2005, 2006). It is extended, with a radius of  $\sim 12'$ .

The Galactic TeV sources with firm associations include high-mass X-ray binaries (HMXBs), supernova remnants (SNRs), and pulsar wind nebulae (PWNe), and they can be point-like (mostly HMXBs) or extended (mostly SNRs and PWNe, Kargaltsev et al. 2007; Hinton & Hofmann 2009). Extragalactic TeV sources are currently represented only by active galactic nuclei (AGN) and appear point-like, except the starburst galaxies, M 82 and NGC 253, whose TeV emission was also observed but could not be resolved by current instruments (Acero et al. 2009; Acciari et al. 2009). HESS J1804-216 is most likely a Galactic source, considering its extended nature and low Galactic latitude. It has several possible associations suggested, though none of them are very compelling. One candidate is the large (with a size of  $\sim 45'$  in radio) and low-surface-brightness SNR G8.7-0.1 (Kassim & Weiler 1990), as HESS J1804-216 has some overlap with the southwestern part of its shell (Aharonian et al. 2006). Another candidate is the young Vela-like pulsar PSR J1803-2137 (the spin period is 134 ms, Clifton & Lyne 1986), which is  $\sim 11'$  away from the best-fit position of HESS J1804-216. Ajello et al. (2012) reported two GeV sources (their sources E and W) detected with the *Fermi* Large Area Telescope (LAT) around HESS J1804-216 but found that they do not match with the TeV source in morphology or spectrum. Instead, their source E has most emission positionally coincident with SNR G8.7-0.1.

Although both SNR G8.7-0.1 and PSR J1803-2137 are also X-ray sources beside their radio emission, there are other X-ray sources that are positionally closer to HESS J1804-216 than them. Bamba et al. (2007) reported detection of two highly absorbed hard X-ray sources with *Suzaku*, i.e., Suzaku J1804-2142 (our Src 1 below) and Suzaku J1804-2140 (our Src 2 below), only  $\sim 2'$  away from the best-fit position of HESS J1804-216 and suggested them as the plausible X-ray counterparts to this TeV source. Kargaltsev et al. (2007) analyzed the *Chandra* observation of these two X-ray sources (CXOU J180441.9-214224 and CXOU J180432.4-214009, respectively) and obtained similar results.

---

<sup>1</sup><http://tevcat.uchicago.edu/>

In Lin et al. (2012, LWB12 hereafter), we carried out source type classifications of 4330 sources from the 2XMMi-DR3 catalog (Watson et al. 2009), which is based on *XMM-Newton* pointed observations. In that project, we serendipitously discovered a 2.93 hr X-ray periodicity from Src 1 and a strong but narrow Fe emission line from Src 2 from three *XMM-Newton* observations of the central part of HESS J1804-216. In this work, after excluding Src 1 and Src 2 as the X-ray counterparts to HESS J1804-216, we search for other possible counterparts in the field of view (FOV), using the source type classification scheme from LWB12.

In Section 2, we describe the screening of spurious sources along with detailed spectral and timing analysis of the relatively bright sources that we selected for final study. In Section 3, we present the results of the source classification and the detailed properties of the sources. In Section 4, we discuss the possible nature of the sources and the possible X-ray counterparts to HESS J1804-216. The conclusions of our study are given in Section 5.

## 2. DATA ANALYSIS

### 2.1. Source Detection and Screening

The three *XMM-Newton* observations that covered the central part of HESS J1804-216 are 0503170101, 0503170201 and 0503170301. They will be referred to as Obs 1, 2, and 3, respectively. Obs 1 was made on 2007 October 2, lasting for about 54 ks, while Obs 2–3 were made only six days later, i.e., 2007 October 8–9, lasting for about 31 ks each. These three observations had the same pointing direction, and the three European Photon Imaging Cameras (EPIC), i.e., pn, MOS1/M1, and MOS2/M2 (Jansen et al. 2001; Strüder et al. 2001; Turner et al. 2001), all used the “medium” optical blocking filter and the “full frame” imaging mode. The X-ray image combined from all these observations and the corresponding FOV relative to observations in other wavelengths are shown in Figure 1.

Sources detected from these three observations are included in the 2XMMi-DR3 catalog, with 524 in total. We found from visual inspection that the catalog has successfully included all significant sources. However, there are also many spurious sources because they appear in the straylight structures (see the bright arcs and the blue stripes in the EPIC image in Figure 1) caused by single reflections of a bright X-ray source outside the FOV. There are also other spurious sources due to problems of low-energy noise near the central line in the pn camera (such sources are detected only in the pn image and only below 0.5 keV) and noisy CCDs in both MOS cameras (such sources tend to be detected as extended in the 2XMMi-DR3 catalog) in all three observations. Because the straylight structures tend not to completely match in sky position in different cameras and noisy CCDs are camera

specific, the spurious sources caused by these problems can show no emission in cameras that are free of these problems at the position of the sources, which can be used to confirm their spurious nature. We find from visual screening that about 150 sources are probably real. However, most of them are faint and have low statistics, making it difficult to study their source properties. Thus in this study we only concentrate on 38 sources that have the signal-to-noise ratio  $S/N > 8$ , or  $S/N > 5$  if they are within  $3'$  from the best-fit position of HESS J1804-216, in at least one observation (Table 2). Our numbering of these sources is given in Figure 1 and Table 2.

We followed the procedure in LWB12 to search for the optical and IR counterparts to these 38 sources in the USNO-B1.0 Catalog (Monet et al. 2003) and the 2MASS Point Source Catalog (2MASS PSC, Cutri et al. 2003) and calculated their X-ray-to-optical and X-ray-to-IR flux ratios, respectively (Table 2). The counterpart is chosen to be the closest one within  $2''$  or three times the X-ray positional error, whichever is larger. We also followed the LWB12 procedure to fit the spectra created from the band count rates included in the 2XMMi-DR3 catalog with an absorbed powerlaw (PL), in order to roughly characterize the spectral shape of the sources.

## 2.2. Detailed Spectral and Timing Analysis

We created light curves for each source and visually searched for stellar X-ray flares to help the source classification. We used SAS 11.0.0 and the calibration files of 2011 June to reprocess the X-ray event files and do the follow-up analysis. Very short intervals of strong background flares occurred in the pn camera in all three observations and were excluded following the SAS thread for filtering high background. The final pn/MOS1/MOS2 exposures used are 46/54/54, 22/31/31, and 25/32/32 ks for Obs 1-3, respectively. For all sources, we used a circular source region centered on the source (the radii used for Src 1 and Src 2 are  $15''$  and  $20''$ , respectively; for others, see Figure 5). The background was estimated from a large circular region, typically with a radius of  $50''$ – $100''$ , near the source in each camera. The event selection criteria followed the default values in the pipeline (see Table 5 in Watson et al. (2009)).

We carried out detailed spectral fitting and timing analysis for sources that we find to be possibly compact object systems containing a white dwarf (WD), a neutron star (NS), or a stellar-mass black hole (BH). As their spectra are in general hard, we only used an absorbed PL to fit their continuum. To improve the statistics and considering that Obs 2 and Obs 3 are relatively short and close in time (in one day), the spectra of both observations were added together for each camera. We rebinned the spectra to have at least 20 counts in each

bin so as to adopt the  $\chi^2$  statistic for the spectral fits.

To search for X-ray periodicity, we created the Leahy power (Leahy et al. 1983) from the light curves that combined all EPIC cameras and were extracted from the source region. We used a binsize of 2.6 s (the frame readout time of the MOS cameras). Although the pn camera has a higher time resolution (73.4 ms) and using data exclusively from this camera allows to search for periodicities at higher frequencies, we found no powers above a 99.9% confidence level at high frequencies. Thus only results using light curves binned at 2.6 s and combining all EPIC cameras will be shown.

To constrain the values of their periods and examine the profiles of the modulation, we employed the epoch folding search technique. The phase folded background-subtracted light curve was obtained by subtracting the folded light curve from the background region (after being rescaled to the size of the source region) from the folded light curve from the source region combining all EPIC cameras.

### 3. RESULTS

#### 3.1. X-ray Properties of Src 1

The spectra of Src 1 are well fitted with an absorbed PL model with photon indices  $\Gamma_{\text{PL}} \sim 1.0$  and the column density  $N_{\text{H}} \sim 10^{22} \text{ cm}^{-2}$  (Table 1). The average flux in Obs 1 is slightly higher (a few tens of percent) than that in Obs 2–3.

The timing properties of Src 1 are shown in Figure 2, and we see strong powers at a period of  $P_0 \approx 10531 \text{ s}$  (i.e., 2.93 hr) and its harmonics (especially  $P_0/3$ ) in both Obs 1 and Obs 2–3. Such a periodic behavior can also be seen in the light curves in the same figure. The pulse profile shows double peaks with comparable maxima and does not seem to vary over the observations (Figure 2). The count rate is consistent with zero in the two low phases, with one lasting for about one third of the period and the other very brief ( $\sim 3\%$  of the period). The pulse profile seems to vary slightly with energy.

#### 3.2. X-ray Properties of Src 2

The fits to the spectra of Src 2 with an absorbed PL show strong residuals around the Fe line energy 6–7 keV (Figure 3), resulting in high values of  $\chi^2_{\nu}$  ( $\sim 1.5$ , Table 1). Thus we added a Gaussian line to the fits. We saw no significant variation of the line centroid energy  $E_{\text{Ga}}$  and FWHM  $\sigma_{\text{Ga}}$  between Obs 1 and Obs 2–3. Thus we chose to tie these parameters to

be the same in these observations in the final fits, to have better constraints on them. We obtained good fits with small photon indices ( $\sim 0.7$ ) and large equivalent widths (EWs) of the Fe line ( $\sim 0.8$  keV) in both Obs 1 and Obs 2–3 (Table 1 and Figure 3).

The timing properties of Src 2 are shown in Figure 4. We see large variability of the source on timescales of about ten hours. The epoch folding search technique suggests a  $\sim 11.4$  hr period (Figure 4), which, however, needs to be confirmed with longer observations.

### 3.3. Properties of Other Sources

The results of multi-wavelength cross-correlation and simple X-ray spectral fits are given in Table 2. Optical and IR counterparts were found for most of the 38 sources. The light curves of 14 sources with some flaring activity are shown in the bottom panels of Figure 5. Stellar flares tend to show a fast rise and a slow decay, as we see in sources like Src 7, 18, and 25, while most of the others do not have such a structure but only exhibit the rise or the decay, due to observation gaps. In LWB12, sources with the X-ray-to-IR flux ratio logarithm  $\log(F_X/F_{\text{IR}})$  (Table 2) less than  $-0.9$  and/or with stellar X-ray flares are classified as stars. Following this scheme, we have 32 candidate stars, based on Table 2 and Figure 5. These stars generally have very soft X-ray spectra ( $\Gamma_{\text{PL}} \gtrsim 4$  in Table 2) and thus mostly appear green in the X-ray colored image in Figure 1. Their spectra become harder when there are stellar flares in the light curves. Some sources (e.g., Src 4–7) were detected because of flares.

The other six sources (Src 1, 2, 27, 30, 34 and 36) are candidate compact objects. We ruled them out as being AGN, considering that they appear in the Galactic plane and that their X-ray spectra are hard (LWB12). Src 27 is PSR J1803-2137. Similar to Src 1 and Src 2, we calculated the Leahy powers for the latter four sources but found no strong power above the 99.9%-confidence level in the frequency range of  $10^{-5}$ – $0.5$  Hz. The light curves, plotted in Figure 5, exhibit little variability. We note that for PSR J1803-2137 we did not use the pn data because the source falls across the CCD gap and near the bright arc (Figure 1) in all observations.

We also carried out detailed spectral fits for these sources. The results are given in Table 1. Src 30, 34 and 36 are all hard ( $\Gamma_{\text{PL}} \lesssim 1$ ) and heavily absorbed ( $N_{\text{H}} \sim 5 \times 10^{22}$   $\text{cm}^{-2}$ ). For Src 34 and Src 36, adding a narrow Fe line improves the fits, similar to Src 2.

In Figure 1, many other (fainter) point sources can be seen. Most of them appear green (thus soft) and are probably stars. We note that the 2XMMi-DR3 catalog also includes 113 extended sources (with the extent radius greater than  $6''$  in at least one of the three observations). However, they are all probably spurious, because most of them appear in the

straylight structures, while others (typically with S/N around 5) seem to be caused by noisy MOS CCDs or bright sources. Thus none of these extended sources are included in our 38 sources.

## 4. DISCUSSION

### 4.1. Comparison with Previous X-ray Study of Src 1 and Src 2

There are studies of observations of the field around HESS J1804-216 by other X-ray observatories. Here we briefly compare their results with ours, focusing on the properties of Src 1 and Src 2. In the *Chandra* 2005-05-04 observation, Kargaltsev et al. (2007) saw a weak and possibly extended/multiple source (CXOU J180441.9-214224) with a size of  $1.5' - 2'$  and the centroid only  $3''$  away from Src 1. They also found the source CXOU J180432.4-214009, which has a 95% positional error of  $1''.4$  and is only  $0''.9$  away from Src 2, based on the position information from the *Chandra* Source Catalog (release 1.1, Evans et al. 2010). In the *Swift* 2005-11-03 observation (12 ks) studied by Landi et al. (2006), no source near Src 1 was detected above  $3\sigma$ , but they found a source (their Src 3 (Sw3 hereafter), with a positional error of  $5'' - 7''$  away from Src 2. In the *Suzaku* 2006-04-06 observation (40 ks), Bamba et al. (2007) found two sources, Suzaku J1804-2142 and Suzaku J1804-2140,  $34''$  and  $23''$  away from Src 1 and Src 2, respectively (the *Suzaku* systematic positional uncertainty is  $1'$ ), with Suzaku J1804-2140 claimed to be extended/multiple. Based on the positional coincidence, CXOU J180441.9-214224 and Suzaku J1804-2142 are probably the same source as Src 1, and CXOU J180432.4-214009, Sw3, and Suzaku J1804-2140 are probably the same source as Src 2. Considering that both Src 1 and Src 2 are point-like with the extent radius  $< 6''$  from the 2XMMi-DR3 catalog, which is supported by the large X-ray modulations on timescales of hours seen in both sources, the extended/multiple feature of CXOU J180441.9-214224 and Suzaku J1804-2140 are probably due to contamination emission from nearby stars or noisy background. For CXOU J180441.9-214224, the contaminating source could be the flaring star Src 6 ( $34''$  away from Src 1), and for Suzaku J1804-2140, it could be the bright star Src 11 ( $\sim 1'$  away from Src 2), which seems to be persistent and has no flare observed by us.

The fluxes of the candidate counterparts to Src 1 and Src 2 estimated by the above studies are within a factor of about two of those that we obtained here, indicating a fairly constant flux level for both sources over about two years. This is not in conflict with the non-detection of Src 1 in the *Swift* 2005-11-03 observation, considering that this observation only detected Src 2, which has a flux five times more than Src 1, at only  $4\sigma$ . Bamba et al. (2007) fitted the spectrum of Suzaku J1804-2142 with an absorbed PL and inferred a harder spectrum ( $\Gamma_{\text{PL}} = -0.3 \pm 0.5$ ) than Src 1, but this could be caused by background contami-

nation, which could be a serious issue due to the low statistics of Suzaku J1804-2142. The fit of CXOU J180432.4-214009 by Kargaltsev et al. (2007) and that of Suzaku J1804-2140 by Bamba et al. (2007) using an absorbed PL both inferred an absorption column density and a photon index with large error bars but fully consistent with those that we obtained for Src 2. We note that Kargaltsev et al. (2007) and Bamba et al. (2007) did not need an Fe line in their spectral fits, probably due to the low statistics of their data. Concerning the timing properties, Kargaltsev et al. (2007) found a 106 s period candidate at only  $2.3\sigma$  for CXOU J180432.4-214009, which we were unable to confirm in either Obs 1 or Obs 2–3 of Src 2 (Figure 4). It could be because this periodicity is not real or is intermittent.

#### 4.2. Nature of Src 1, 2, 30, 34 and 36

Considering that the Galactic TeV sources with firm associations are mostly HMXBs, SNRs and PWNe, Bamba et al. (2007) and Kargaltsev et al. (2007) discussed both Src 1 and Src 2 in terms of these source types as the X-ray counterparts to HESS J1804-216. However, the large X-ray modulation on timescales of hours observed by us in these two sources excludes them from being SNRs or PWNe.

It is unlikely that Src 1 is a HMXB for several reasons. Its 2.93 hr X-ray period is too short to be the orbital period, because HMXBs mostly have orbital periods longer than one day (Bildsten et al. 1997; Charles & Coe 2006) (but this cannot exclude it as a low-mass X-ray binary like the pulsar Her X-1). This period seems too long to be the NS spin period either (the slowest pulsar known is RX J0146.9+6121, with a spin period of 1412 s (Hellier 1994)). It has a long low phase in the pulse profile, which is rarely seen in HMXBs (e.g., Bildsten et al. 1997). Its 0.3–10.0 keV unabsorbed luminosity is about  $10^{33}$  erg s<sup>-1</sup> (assuming a source distance of 8 kpc), which is too low for accretion-powered X-ray pulsars (typically higher than  $10^{34}$  erg s<sup>-1</sup>, Munro et al. 2004). Considering the low luminosity and the hard spectra, we suggest Src 1 to be a magnetic cataclysmic variable (CV; polar or intermediate polar). The 2.93 hr period could be either the orbital period or the spin period of the WD (they are the same for polars). Further, the observed pulse profile is similar to those of some eclipsing polars at high energies (above 1 keV), e.g., the eclipsing polar HU Aquarii (See Figure 3 in Schwarz et al. 2009). The light curve would then be dominated by a single bright phase interval (phase 0.2–0.8 in Figure 2) of a self-eclipsing pole, with the short low period (phase around 0.6) caused by the eclipse of the accretion region by the secondary star. We checked whether an Fe emission line is present in the spectra of Src 1 by adding a Gaussian emission line to the spectral fits, considering that magnetic CVs often exhibit Fe emission lines with EWs typical of a few hundred eV (Ezuka & Ishida 1999). We found



that adding the line did not improve the fits (the total  $\chi^2$  values decreased by less than 2 for both Obs 1 and Obs 2-3), but we also obtained very high EW upper limits ( $\sim 1.4$  keV, at a 90% confidence level). Thus we cannot rule out the presence of Fe emission lines in Src 1 at the level often seen in magnetic CVs.

Src 2 has a 0.3–10.0 keV unabsorbed luminosity of about  $6 \times 10^{33}$  erg s $^{-1}$ , assuming a source distance of 8 kpc. Such a luminosity also seems low for a HMXB. Its Fe emission line is also stronger than most HMXBs ( $EW \lesssim 100$  eV, Munro et al. 2004), while it is close to typical values seen in magnetic CVs (Ezuka & Ishida 1999). In fact, sources with an X-ray luminosity, a hard spectrum, and a strong Fe emission line like Src 2 are commonly seen toward the Galactic center, and Munro et al. (2004) argued that they are most likely intermediate polars. Src 2 is probably one such object.

Src 30, 34 and 36 have similar low luminosities (also assuming a distance of 8 kpc) and hard spectra like Src 1 and Src 2. Thus they are probably magnetic CVs too. Although they have steady light curves and may be rotation-powered pulsars like PSR J1803-2137, we do not favor this interpretation because the rotation-powered pulsars tend to have  $\Gamma_{\text{PL}} \gtrsim 1$  (Munro et al. 2004, LWB12).

### 4.3. The X-ray Counterpart to HESS J1804-216

If Src 1 and Src 2 are CVs, they are unlikely to be the counterparts to HESS J1804-216. Src 30, 34 and 36 are far away (more than 12') from HESS J1804-216 and are unlikely to be its counterparts either. The promising counterpart candidates are the SNR G8.7-0.1 and PSR J1803-2137 (i.e., Src 27), although they are not positionally close to this TeV source (Aharonian et al. 2006). Ajello et al. (2012) explained the GeV and TeV  $\gamma$ -ray emission in terms of the interaction between G8.7-0.1 and adjacent (for GeV emission) or distant (for TeV emission) molecular clouds (Blitz et al. 1982), which is supported by the detection of a single bright OH(1720 MHz) maser in the eastern edge of G8.7-0.1 by Hewitt & Yusef-Zadeh (2009).

*ROSAT* detected extended thermal X-ray emission from the northeastern part of G8.7-0.1, with a temperature of 0.3–0.7 keV and a column density of  $(1.2\text{--}1.4) \times 10^{22}$  cm $^{-2}$  (Finley & Oegelman 1994). Puehlhofer et al. (2011) obtained consistent results and supported the thermal nature of the extended X-ray emission using the *XMM-Newton* observation 0405750201 (exposure 16 ks). The X-ray image of this observation is shown in Figure 6 (available in the electronic version of the article), in which the extended thermal emission appears in green. There is no clear extended hard emission other than the straylight, which is also seen in this observation,

and the small extended source near PSR J1806-2125 (the magenta plus in Figure 6), which has an extent radius of only  $21.1 \pm 0.7''$  from the 2XMMi-DR3 catalog. This extended emission was suggested to be a new PWN unassociated with PSR J1806-2125 by Puehlhofer et al. (2011).

In spite of six times more exposure, Obs 1-3 failed to detect extended thermal X-ray emission as seen in observation 0405750201. This could be due to spatial variation in absorption, which, however, was not supported by Finley & Oegelman (1994), because they observed no significant spatial correlation between the intensity and the hardness ratio of the X-ray emission. Alternatively, X-ray emission from the SNR can be intrinsically very weak, considering its low surface brightness.

Ajello et al. (2012) could not rule out the possibility that the TeV emission is from the inverse Compton scattering of the relativistic electrons in a PWN associated with sources such as PSR J1803-2137 and Suzaku J1804-2140 (i.e., our Src 2). We have argued that Src 2 is not a PWN. PSR J1803-2137 is extended but has a diameter size of only  $\sim 7''$  from the *Chandra* observation (Cui & Konopelko 2006). This size is too small to be resolved by *XMM-Newton*. The spectral parameters that we obtained from the *XMM-Newton* observations are fully consistent with those obtained by Cui & Konopelko (2006), indicating little long-term X-ray variability. This is expected for rotation-powered pulsars (LWB12). The short-term variability is small too (Figure 5), as expected for an extended source. Cui & Konopelko (2006) suggested that PSR J1803-2137 is a PWN, whose X-ray emission probably just reflects the bright core of the (large) PWN. We note that PSR J1803-2137 was suggested to be associated with G8.7-0.1 (Kassim & Weiler 1990), but this was not supported by the proper motion of PSR J1803-2137 measured by Brisken et al. (2006), which indicates a birth position at the extreme edge of the SNR.

## 5. CONCLUSIONS

We have studied three *XMM-Newton* observations of the central part of the unidentified TeV  $\gamma$ -ray source HESS J1804-216. We focus on two X-ray sources (Src 1 and Src 2) that were suggested to be the counterparts to the TeV source. Src 1 is probably an eclipsing polar, based on our discovery of a 2.93 hr X-ray periodicity from this source and the pulse profile that can be naturally explained by a self-eclipsing pole. We detect a strong Fe emission line (FWHM  $\sim 0.3$  keV and EW  $\sim 0.8$  keV) and strong X-ray variability on timescales of hours from Src 2. This source is probably an intermediate polar, which is often seen in the Galactic center. Thus Src 1 and Src 2 are probably two magnetic CVs that happen to be in the direction of the TeV source, not its X-ray counterparts.

We carry out systematic classification of 38 relatively bright sources and find three new compact object systems, in addition to Src 1, Src 2 and PSR J1803-2137. Others are probably normal stars. The new compact object systems are probably CVs too, and they are far away from HESS J1804-216, thus unlikely to be its X-ray counterparts either. HESS J1804-216 is still most likely associated with SNR G8.7-0.1 or PSR J1803-2137, as suggested before. No clear extended emission is observed, confirming that G8.7-0.1 only has bright thermal emission in its northeastern shell. PSR J1803-2137 shows little long-term X-ray variability compared with previous studies and cannot be resolved by *XMM-Newton*, indicating an extent radius  $<6''$ .

Acknowledgments: We thank the anonymous referee for the helpful comments. We acknowledge the use of public data from the *XMM-Newton* data archive and the 2XMM Serendipitous Source Catalog, constructed by the XMM-Newton Survey Science Center on behalf of ESA.

## REFERENCES

- Acciari, V. A., Aliu, E., Arlen, T., et al. 2009, *Nature*, 462, 770
- Acerro, F., Aharonian, F., Akhperjanian, A. G., et al. 2009, *Science*, 326, 1080
- Aharonian, F., Akhperjanian, A. G., Aye, K.-M., et al. 2005, *Science*, 307, 1938
- Aharonian, F., Akhperjanian, A. G., Bazer-Bachi, A. R., et al. 2006, *ApJ*, 636, 777
- Ajello, M., Allafort, A., Baldini, L., et al. 2012, *ApJ*, 744, 80
- Bamba, A., Koyama, K., Hiraga, J. S., et al. 2007, *PASJ*, 59, 209
- Bildsten, L., Chakrabarty, D., Chiu, J., et al. 1997, *ApJS*, 113, 367
- Blitz, L., Fich, M., & Stark, A. A. 1982, *ApJS*, 49, 183
- Brisken, W. F., Carrillo-Barragán, M., Kurtz, S., & Finley, J. P. 2006, *ApJ*, 652, 554
- Brogan, C. L., Gelfand, J. D., Gaensler, B. M., Kassim, N. E., & Lazio, T. J. W. 2006, *ApJ*, 639, L25
- Charles, P. A. & Coe, M. J. 2006, *Optical, ultraviolet and infrared observations of X-ray binaries*, ed. W. H. G. Lewin & M. van der Klis, 215–265

- Clifton, T. R. & Lyne, A. G. 1986, *Nature*, 320, 43
- Cui, W. & Konopelko, A. 2006, *ApJ*, 652, L109
- Cutri, R. M., Skrutskie, M. F., van Dyk, S., et al. 2003, *VizieR Online Data Catalog*, 2246, 0
- Evans, I. N., Primini, F. A., Glotfelty, K. J., et al. 2010, *ApJS*, 189, 37
- Ezuka, H. & Ishida, M. 1999, *ApJS*, 120, 277
- Finley, J. P. & Oegelman, H. 1994, *ApJ*, 434, L25
- Hellier, C. 1994, *MNRAS*, 271, L21
- Hewitt, J. W. & Yusef-Zadeh, F. 2009, *ApJ*, 694, L16
- Hinton, J. A. & Hofmann, W. 2009, *ARA&A*, 47, 523
- Jansen, F., Lumb, D., Altieri, B., et al. 2001, *A&A*, 365, L1
- Kargaltsev, O., Pavlov, G. G., & Garmire, G. P. 2007, *ApJ*, 670, 643
- Kassim, N. E. & Weiler, K. W. 1990, *ApJ*, 360, 184
- Landi, R., Bassani, L., Malizia, A., et al. 2006, *ApJ*, 651, 190
- Leahy, D. A., Darbro, W., Elsner, R. F., et al. 1983, *ApJ*, 266, 160
- Lin, D., Webb, N. A., & Barret, D. 2012, *ApJ*, 756, 27
- Monet, D. G., Levine, S. E., Canzian, B., et al. 2003, *AJ*, 125, 984
- Muno, M. P., Arabadjis, J. S., Baganoff, F. K., et al. 2004, *ApJ*, 613, 1179
- Puehlhofer, G., Frech-Horn, T., Sasaki, M., & Klochkov, D. 2011, in *The X-ray Universe 2011*, ed. J.-U. Ness & M. Ehle, 269
- Schwarz, R., Schwobe, A. D., Vogel, J., et al. 2009, *A&A*, 496, 833
- Strüder, L., Briel, U., Dennerl, K., et al. 2001, *A&A*, 365, L18
- Turner, M. J. L., Abbey, A., Arnaud, M., et al. 2001, *A&A*, 365, L27
- Watson, M. G., Schröder, A. C., Fyfe, D., et al. 2009, *A&A*, 493, 339

Table 1. Spectral fits of candidate compact objects

Src	Obs	$N_{\text{H}}$ ( $10^{22} \text{ cm}^{-2}$ )	$\Gamma_{\text{PL}}$	$N_{\text{PL}}$ ( $10^{-5}$ )	$E_{\text{Ga}}$ (keV)	$\sigma_{\text{Ga}}$ (keV)	$N_{\text{Ga}}$ ( $10^{-5}$ )	EW (keV)	$\chi^2_{\nu}(\nu)$	$F_{\text{abs}}$ ( $10^{-13} \text{ erg s}^{-1} \text{ cm}^{-2}$ )	$F_{\text{unabs}}$ ( $10^{-13} \text{ erg s}^{-1} \text{ cm}^{-2}$ )
(1)	(2)	(3)	(4)	(5)	(6)	(7)	(8)	(9)	(10)	(11)	(12)
1	1	$1.0^{+0.5}_{-0.4}$	$1.0^{+0.3}_{-0.3}$	$1.1^{+0.8}_{-0.4}$	...	...	...	...	0.93(25)	$1.5^{+0.3}_{-0.2}$	$1.8^{+0.3}_{-0.3}$
	2+3		$1.2^{+0.4}_{-0.4}$	$1.1^{+0.9}_{-0.4}$	...	...	...	...	1.15(21)	$1.0^{+0.2}_{-0.2}$	$1.3^{+0.2}_{-0.2}$
2	1	$5.3^{+1.0}_{-0.9}$	$0.3^{+0.2}_{-0.2}$	$1.8^{+0.9}_{-0.6}$	...	...	...	...	1.65(93)	$6.4^{+0.5}_{-0.5}$	$8.2^{+0.6}_{-0.6}$
	2+3		$0.4^{+0.2}_{-0.2}$	$1.9^{+0.9}_{-0.6}$	...	...	...	...	1.42(83)	$5.3^{+0.5}_{-0.4}$	$6.9^{+0.6}_{-0.5}$
27	1	$5.8^{+1.1}_{-0.9}$	$0.6^{+0.3}_{-0.2}$	$2.7^{+1.6}_{-1.0}$	$6.6^{+0.1}_{-0.1}$	$0.3^{+0.1}_{-0.1}$	$0.8^{+0.2}_{-0.2}$	$1.0^{+0.3}_{-0.3}$	1.02(90)	$6.2^{+0.5}_{-0.4}$	$8.4^{+0.8}_{-0.7}$
	2+3		$0.8^{+0.3}_{-0.3}$	$2.9^{+1.9}_{-1.1}$			$0.5^{+0.2}_{-0.2}$	$0.8^{+0.4}_{-0.3}$	1.11(80)	$5.0^{+0.4}_{-0.4}$	$7.1^{+0.7}_{-0.6}$
30	1	$4.8^{+3.4}_{-2.2}$	$1.0^{+0.3}_{-0.3}$	$1.1^{+0.6}_{-0.4}$	...	...	...	...	0.55(21)	$1.4^{+0.2}_{-0.2}$	$1.7^{+0.2}_{-0.2}$
	2+3		$1.1^{+0.3}_{-0.3}$	$1.1^{+0.5}_{-0.3}$	...	...	...	...	0.71(24)	$1.1^{+0.2}_{-0.2}$	$1.4^{+0.2}_{-0.2}$
34	1	$3.7^{+1.5}_{-1.2}$	$0.3^{+0.7}_{-0.6}$	$0.5^{+1.3}_{-0.3}$	...	...	...	...	0.98(13)	$1.8^{+0.4}_{-0.4}$	$2.3^{+0.5}_{-0.4}$
	2+3		$0.1^{+0.6}_{-0.5}$	$0.4^{+0.7}_{-0.2}$	...	...	...	...	0.89(17)	$2.1^{+0.4}_{-0.4}$	$2.5^{+0.5}_{-0.4}$
36	1	$5.0^{+2.0}_{-1.6}$	$0.4^{+0.4}_{-0.4}$	$1.1^{+1.2}_{-0.5}$	...	...	...	...	1.50(33)	$3.4^{+0.5}_{-0.5}$	$4.2^{+0.6}_{-0.6}$
	2+3		$0.2^{+0.4}_{-0.4}$	$1.1^{+1.1}_{-0.5}$	...	...	...	...	1.07(36)	$4.9^{+0.7}_{-0.7}$	$5.9^{+0.8}_{-0.8}$
36	1	$5.0^{+1.1}_{-0.9}$	$1.1^{+0.6}_{-0.5}$	$3.0^{+5.5}_{-1.8}$	$6.7^{+0.1}_{-0.1}$	$0.3^{+0.1}_{-0.1}$	$0.6^{+0.3}_{-0.3}$	$1.7^{+1.2}_{-0.8}$	1.04(30)	$3.3^{+0.5}_{-0.5}$	$4.8^{+1.9}_{-0.8}$
	2+3		$0.7^{+0.6}_{-0.5}$	$2.3^{+3.6}_{-1.3}$			$0.6^{+0.4}_{-0.3}$	$1.0^{+0.8}_{-0.5}$	0.79(33)	$4.5^{+0.7}_{-0.7}$	$6.2^{+1.3}_{-0.9}$
36	1	$5.5^{+1.2}_{-1.0}$	$0.5^{+0.3}_{-0.2}$	$1.8^{+1.1}_{-0.7}$	...	...	...	...	1.00(63)	$4.9^{+0.5}_{-0.5}$	$6.5^{+0.6}_{-0.6}$
	2+3		$0.8^{+0.3}_{-0.3}$	$3.2^{+1.9}_{-1.1}$	...	...	...	...	1.36(73)	$4.9^{+0.5}_{-0.5}$	$7.0^{+0.8}_{-0.7}$
36	1	$5.5^{+1.2}_{-1.0}$	$0.7^{+0.3}_{-0.3}$	$2.6^{+1.8}_{-1.0}$	$6.7^{+0.1}_{-0.1}$	$0.2^{+0.1}_{-0.1}$	$0.3^{+0.2}_{-0.2}$	$0.4^{+0.3}_{-0.2}$	0.91(60)	$4.8^{+0.5}_{-0.5}$	$6.7^{+0.8}_{-0.7}$
	2+3		$1.1^{+0.4}_{-0.3}$	$5.3^{+4.2}_{-2.2}$			$0.6^{+0.2}_{-0.2}$	$0.9^{+0.5}_{-0.4}$	1.06(70)	$4.8^{+0.5}_{-0.5}$	$7.6^{+1.4}_{-0.9}$

Note. — Columns: (1) our source numbering; (2) the observation; (3) the absorption column density; (4)-(5) the PL photon index and normalization, respectively; (6)-(9) the centroid energy, the FWHM, the normalization, and the equivalent width of the Gaussian emission line, respectively; (10) the reduced  $\chi^2$  ( $\chi^2_{\nu}$ ) and the degrees of freedom ( $\nu$ ); (11)-(12) the 0.3–10.0 keV absorbed and unabsorbed fluxes, respectively. All the fits were made to the 0.3–10.0 keV spectra. Parameters with values shared by both Obs 1 and Obs 2–3 are tied to be the same between these observations.



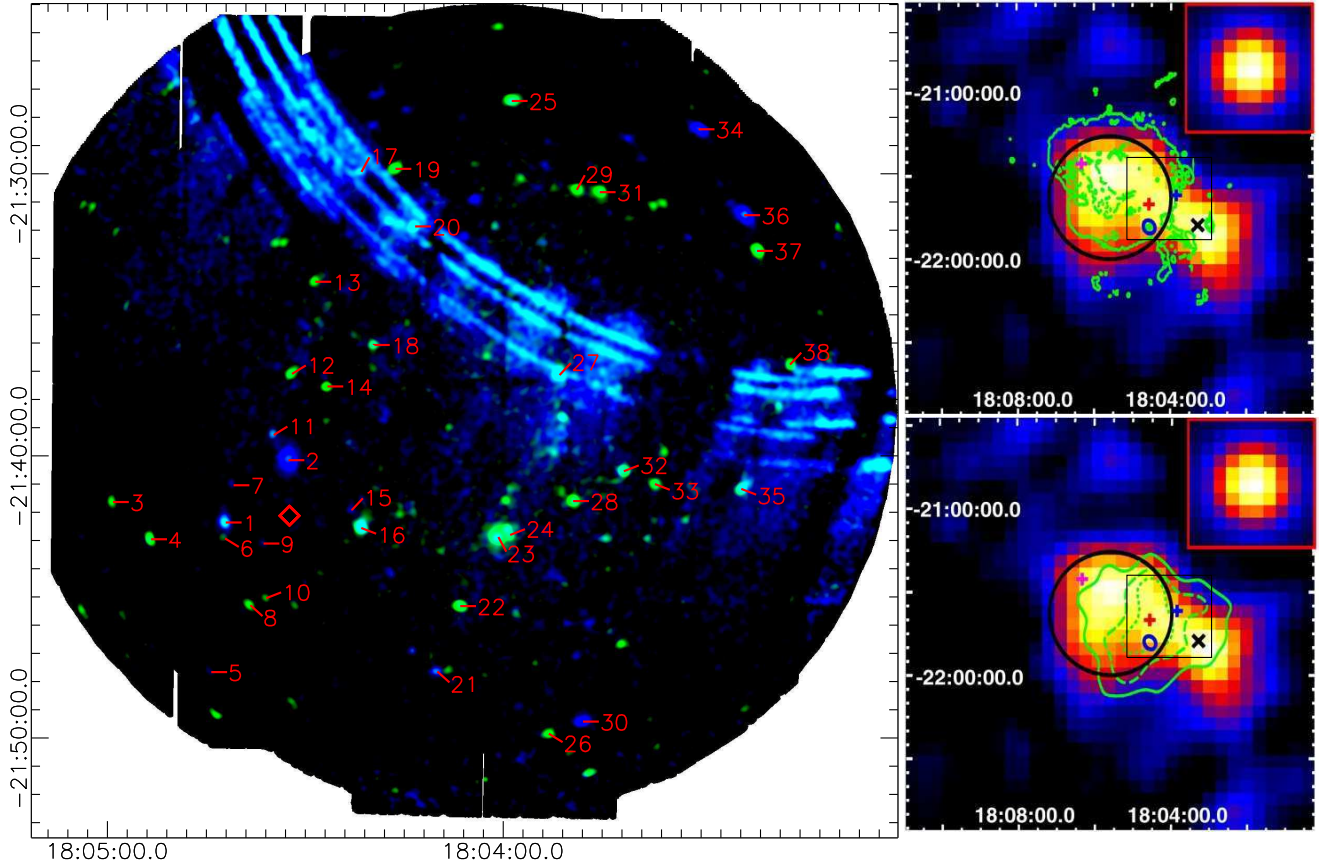


Fig. 1.— (Left panel): The *XMM-Newton* X-ray image of the field around HESS J1804-216. Data from all three EPIC cameras from all three observations were combined. The image is false-colored as follows: 0.5–2.0 keV photons in green and 2.0–12.0 keV photons in blue (We did not include photons at lower energies to avoid low-energy noise). The image has a bin size of  $2'' \times 2$  and is smoothed by a Gaussian kernel of  $\sigma=5''$ . The red diamond marks the best-fit position of HESS J1804-216. The sources studied by us are numbered from the left to the right, except Src 1 and Src 2; see Table 2. (Right panels): The *Fermi* LAT 2–10 GeV map from Ajello et al. (2012), with the green contours indicating the VLA 90 cm image at 5%, 15%, and 25% of the peak intensity (Brogan et al. 2006) in the top panel and the subtracted TeV photon counts of HESS J1804-216 at 25%, 50%, and 75% levels (Aharonian et al. 2006) in the bottom panel. The black box corresponds to the size of the left panel. The black circle indicates the best-fit disk size of Source E in Aharonian et al. (2006), while the black cross is for their Source W. The blue, magenta, and red plus signs indicate PSR J1803-2137 (our Src 27), PSR J1806-2125, and Suzaku J1804-2140 (our Src 2), respectively, while the blue ellipse indicates the radio extension of SNR G8.31-0.09 (Aharonian et al. 2006).

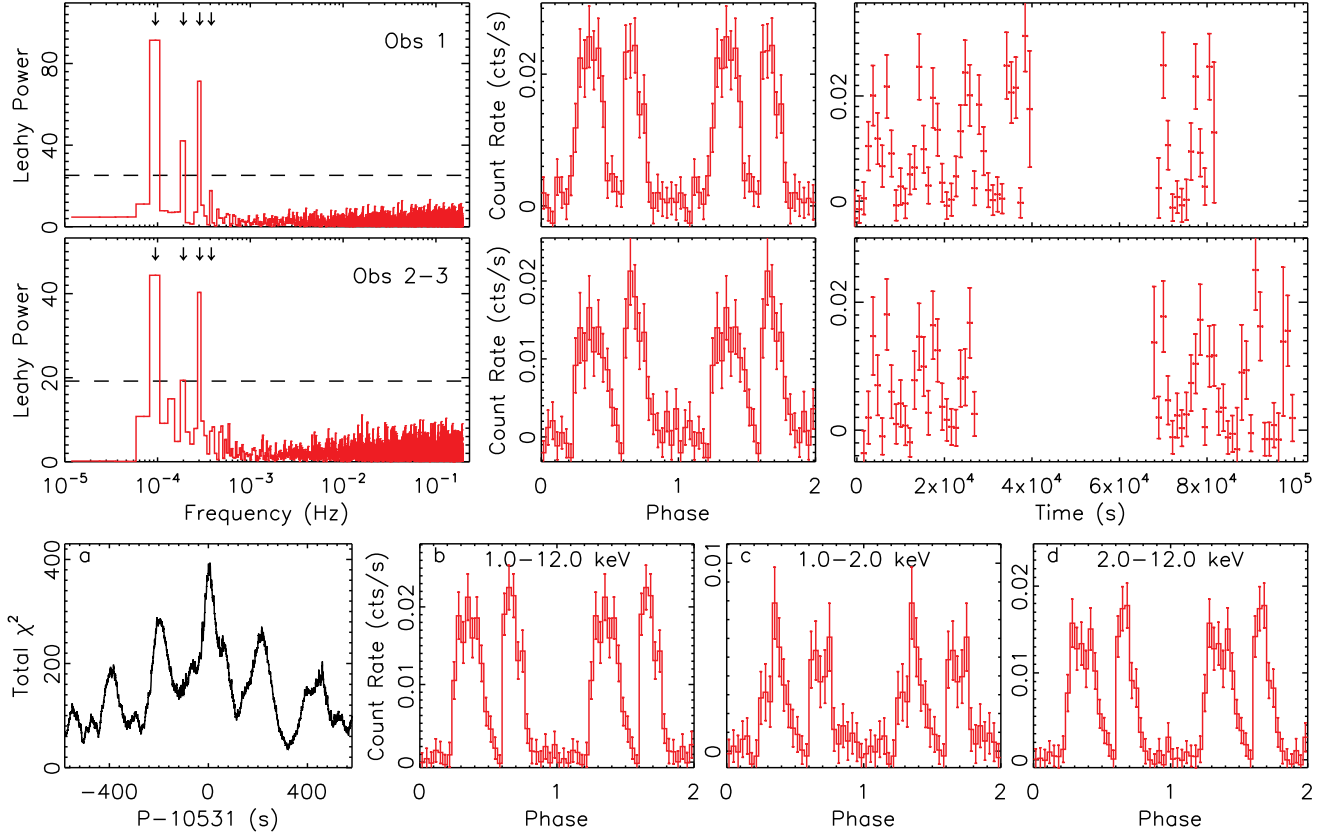


Fig. 2.— The timing properties of Src 1. The panels in the top two rows show the Leahy power (left), the light curve folded at a period of  $P_0=10531$  s (middle), and the (unfolded) light curve (right) for each observation (1.0–12.0 keV). The arrows from the left to the right in the power plots mark the period  $P_0$  and the harmonics  $P_0/2$ ,  $P_0/3$ , and  $P_0/4$ , respectively. The dashed lines indicate a 99.9% confidence detection level. The unfolded light curves are shifted in time to be aligned in phase. Panel (a) in the bottom row shows the total  $\chi^2$  values from the fits to a constant to the 1.0–12.0 keV light curves folded at various tentative periods using all three observations. The 1.0–12.0 keV, 1.0–2.0 keV and 2.0–12.0 keV light curves folded at  $P_0$  also using all three observations are given in panels (b), (c), and (d), respectively.



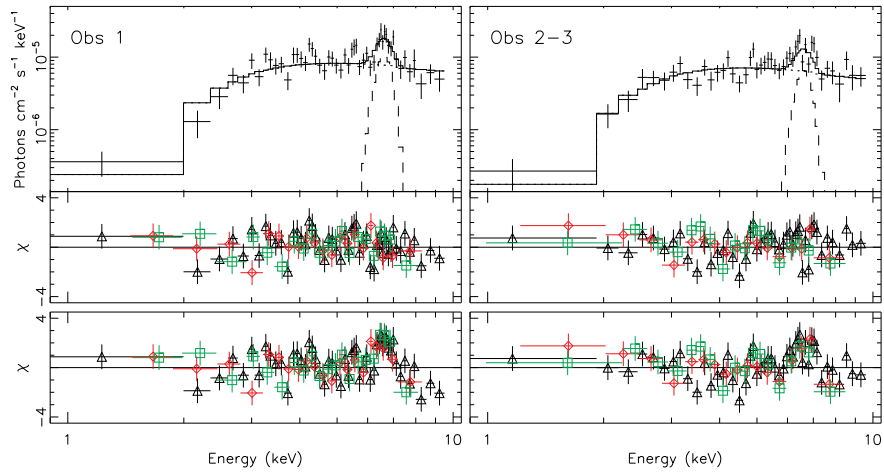


Fig. 3.— The unfolded spectra (top panels) and the fit residuals (middle panels) using an absorbed PL plus a Gaussian Fe line model and the fit residuals using only an absorbed PL (bottom panels) for Src 2. For clarity, only the pn spectra are shown for the unfolded spectra. The dotted, dashed, and solid lines are for the PL and Fe components and the total model, respectively. The residuals are shown for all three cameras (black triangles/red diamonds/green squares for pn/MOS1/MOS2, respectively).

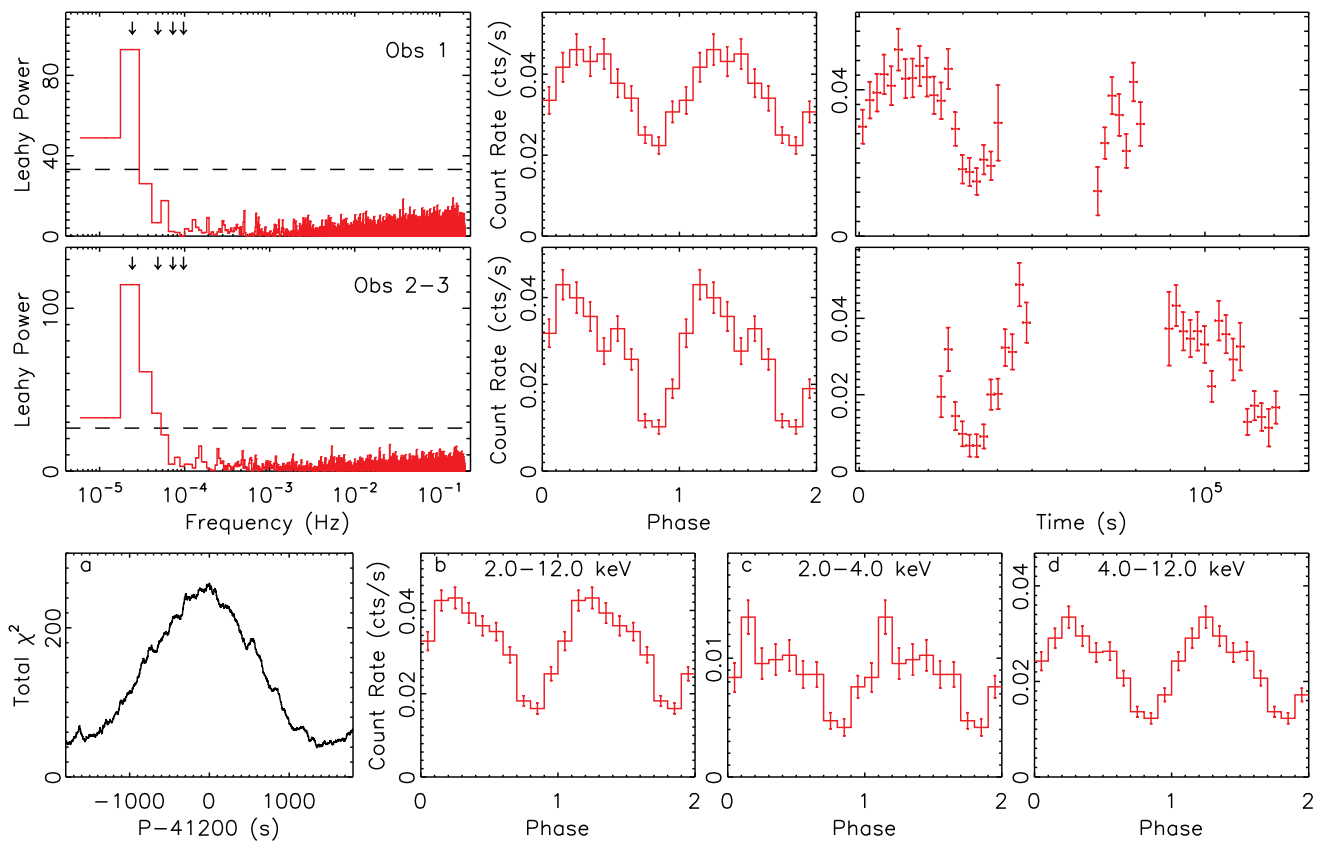


Fig. 4.— The timing properties of Src 2, similar to Figure 2. The energy band 2.0–12.0 keV is used for all plots except panels (c) and (d). The period used for all folded light curves is 41200 s

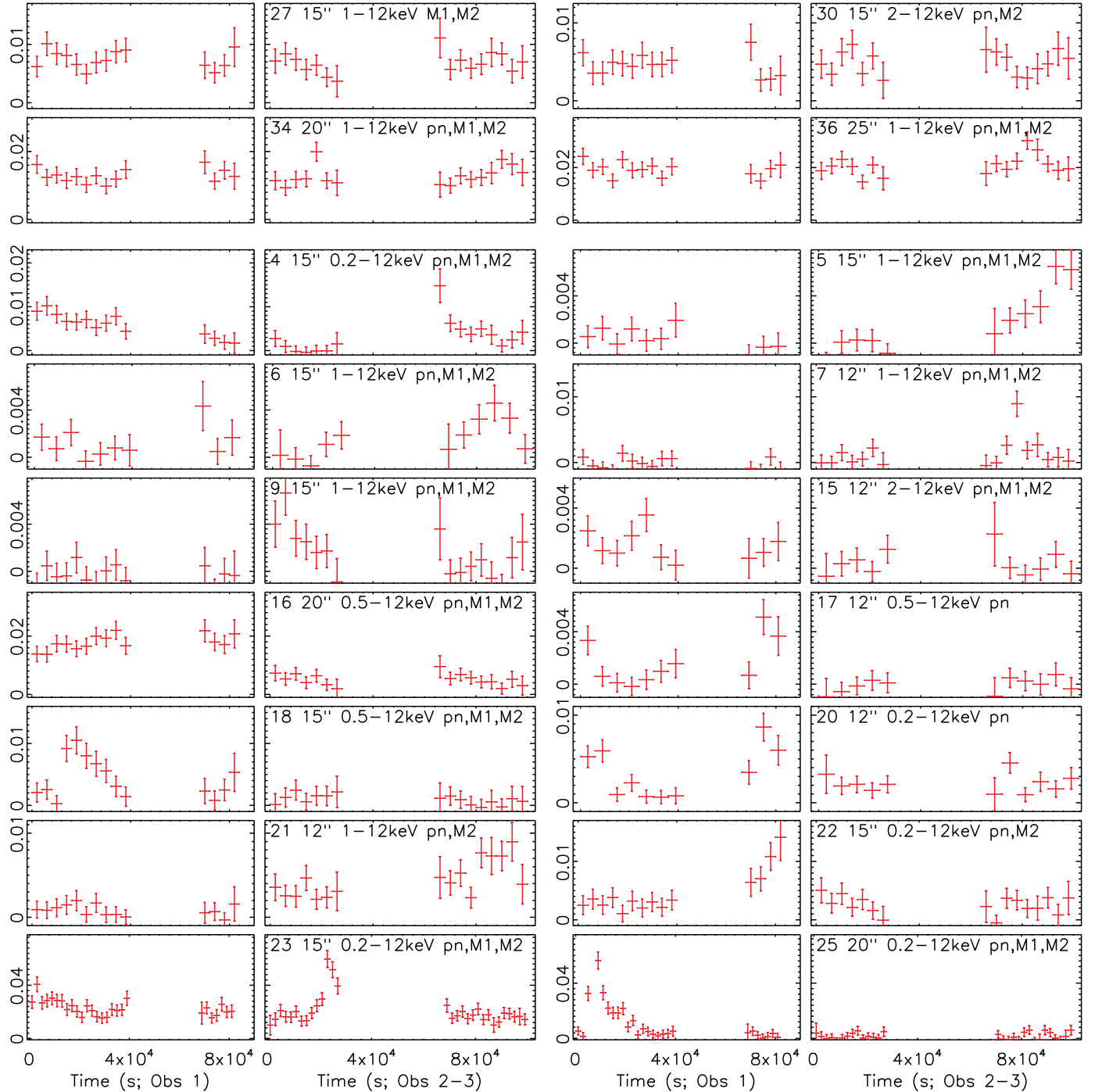


Fig. 5.— The light curves (in units of  $\text{cts s}^{-1}$ ) of candidate compact object systems (the top four sources), which show little short-term variability, and those of stars with some flaring activity (others). The note in the panel containing Obs 2-3 includes the source number, the radius of the source extraction region, the energy band, and the instruments used.

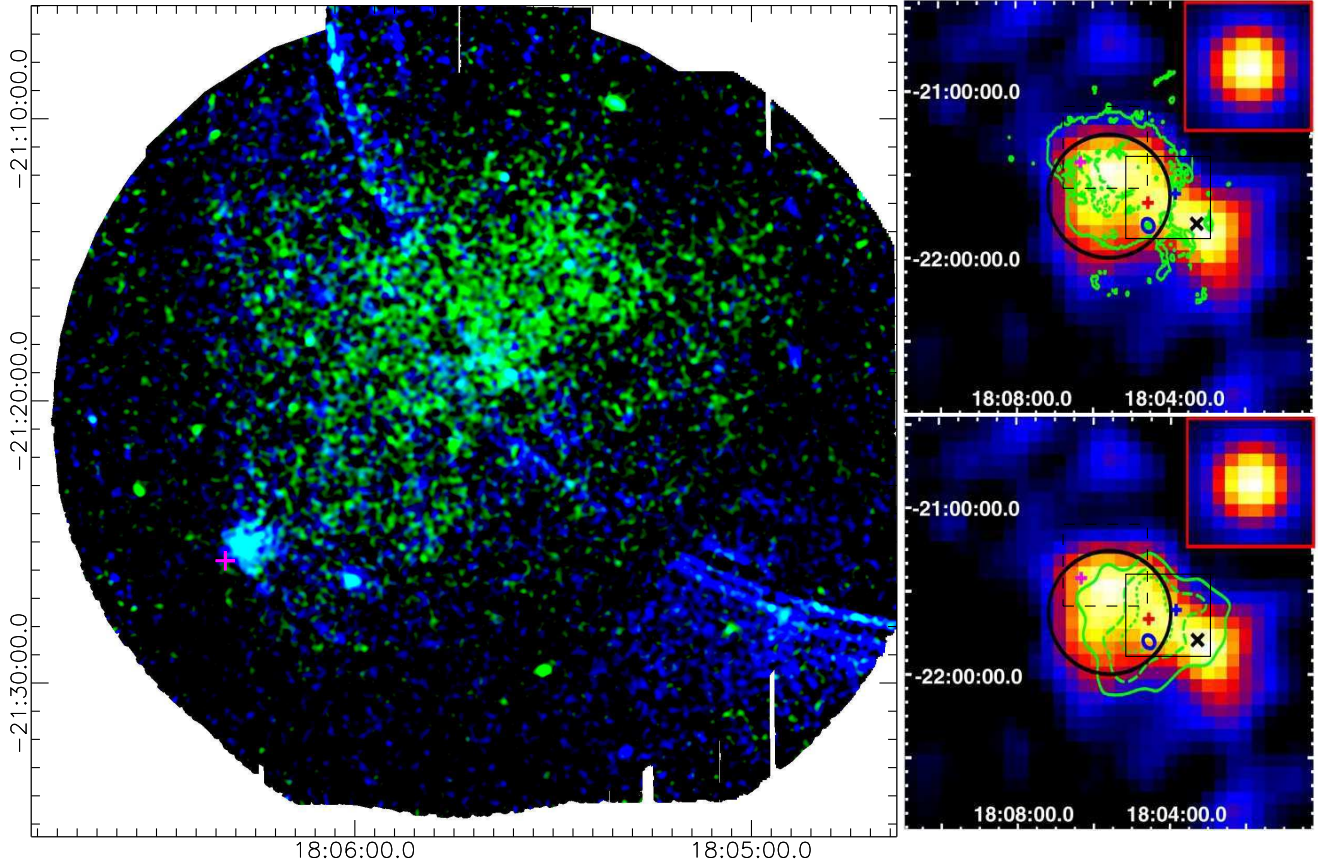


Fig. 6.— The *XMM-Newton* X-ray image of the field around HESS J1804-216, similar to Figure 1, but for observation 0405750201. The black dashed-line and solid-line boxes correspond to the size of the left panel of this figure and that of the left panel of Figure 1, respectively.